Time-reversal of nonlinear waves: Applicability and limitations

G. Ducrozet,[1,*] M. Fink,[2] and A. Chabchoub[3,4]

[1] *LHEEA, École Centrale Nantes, UMR CNRS No. 6598, 1 rue de la Noë, 44321 Nantes, France*

[2] *Institut Langevin, ESPCI Paris, PSL University, CNRS, UMR CNRS No. 7587, 10 rue Vauquelin, 75005 Paris, France*

[3] *Department of Mechanical Engineering, School of Engineering, Aalto University, 02150 Espoo, Finland*

[4] *Department of Ocean Technology Policy and Environment, Graduate School of Frontier Sciences, The University of Tokyo, Kashiwa, Chiba 277-8563, Japan*

(Received 21 March 2016; published 22 September 2016)

Time-reversal (TR) refocusing of waves is one of the fundamental principles in wave physics. Using the TR approach, time-reversal mirrors can physically create a time-reversed wave that exactly refocus back, in space and time, to its original source regardless of the complexity of the medium as if time were going backward. Laboratory experiments have proved that this approach can be applied not only in acoustics and electromagnetism, but also in the field of linear and nonlinear water waves. Studying the range of validity and limitations of the TR approach may determine and quantify its range of applicability in hydrodynamics. In this context, we report a numerical study of hydrodynamic time-reversal using a unidirectional numerical wave tank, implemented by the nonlinear high-order spectral method, known to accurately model the physical processes at play, beyond physical laboratory restrictions. The applicability of the TR approach is assessed over a variety of hydrodynamic localized and pulsating structures' configurations, pointing out the importance of high-order dispersive and particularly nonlinear effects in the refocusing of hydrodynamic stationary envelope solitons and breathers. We expect that the results may motivate similar experiments in other nonlinear dispersive media and encourage several applications with particular emphasis on the field of ocean engineering.

DOI: 10.1103/PhysRevFluids.1.054302

I. INTRODUCTION

Nonlinearity is a fundamental feature of hydrodynamic evolution equations and is therefore crucial for the accurate description of water waves [1,2]. One particular and prominent form of hydrodynamic instability of nonlinear waves is the Benjamin-Feir instability [3]. This instability has been discussed in modeling oceanic extremes. Indeed, the formation of extremely large and steep waves in real seas, also known as freak or rogue waves (RWs), has drawn significant scientific attention (see [4–8]). In fact, the dynamics of RWs can be described and modeled within the framework of exact solutions of the nonlinear Schrödinger equation (NLSE) [9–11]. Further, integrable weakly nonlinear evolution equations, such as the NLSE, allow us to discuss the propagation characteristics of specific and complex waves by means of exact solutions [12,13]. Recent laboratory and numerical studies have confirmed the existence of hydrodynamic breathers [14–16]. Being controllable in both time and space, breathers are more accurate physical models to generate extreme waves for engineering application purposes, rather than using the inefficient and simplified linear superposition principle. Prominent models are, for instance, the family of doubly localized Peregrine and Akhmediev-Peregrine breathers.

The time-reversal (TR) procedure is another fundamental principle in wave physics and it has been used in several contexts in past years, especially for acoustic and elastic waves [17,18]. This TR technique, based on TR mirrors, works as follows: A given wave pulse, generated at a source, is

*guillaume.ducrozet@ec-nantes.fr

then measured by a set of antennas or probes after a certain propagation in space. These signals are then time-reversed and rebroadcasted from the same measurement locations by the TR mirrors. If TR invariance is valid, the initial wave pulse is expected to focus back at the original source location, independently of the complexity of the medium.

The effects of dispersion [18,19] and nonlinearities [20] have been experimentally studied for acoustic waves. It has been shown that the time-reversed field focuses back in time and space as long as nonlinearities do not create dissipation, i.e., as long as the propagation distance is smaller than the shock distance.

Different TR procedures have been experimentally applied in the field of water waves. The TR mirror has been shown to be valid for wave fields with very weak nonlinearity in the configuration of a water tank cavity and multiple mirror reflections [21] and recently, a new concept of instantaneous time mirror has been tested also for water waves [22]. Also, strongly and doubly localized breather solutions have been used to study the time refocusing of nonlinear waves in a unidirectional wave flume [23]. This study has shown that for these RW models, which are steep in amplitude and therefore strongly nonlinear waves, time-reversal is still accurately valid.

In this paper we extend the experimental work [23] and report an extensive and detailed numerical study of the effects of dispersion and nonlinearities on hydrodynamic time-reversal within the framework of NLSE envelope solitons and breathers. The main goal of this work is to accurately quantify the validity of the TR approach for water waves, based on a numerical wave tank (NWT) [24], implemented by the conservative higher-order spectral (HOS) method [25,26]. It is shown that the time-reversal is indeed valid for nonlinear waves for a wide range of wave propagation distances and steepness values. This proves the robustness of the TR property of NLSE localized structures with respect to noise and chaos. Limitations of the TR approach are also discussed in detail. We emphasize that the investigation of the effect of dispersion and nonlinearity on hydrodynamic time-reversal characteristics of focused waves, taking also into account, for instance, bound waves and the inaccuracies of wave maker's wave generation, has been studied within the framework of the Zakharov equation in Ref. [27].

The paper is organized as follows. Section II presents the weakly nonlinear theory of water waves and the TR principle. In Sec. III the NWT configuration will be detailed as well as the method used to generate localized structures inside this NWT. Section IV is devoted to the validity analysis of the time-reversal for water waves in relation to nonlinearity of the wave field as well as to dispersion effects. Section V analyzes the properties of the physical processes, including a discussion on the limitations of the TR method in hydrodynamics.

II. NONLINEAR WAVES AND THE TIME-REVERSAL PRINCIPLE

In this work we are interested in the propagation of water waves at large scales and consequently we limit our study to surface gravity waves. Furthermore, we assume that the waves are evolving in deep water, that is, we assume that the ratio of the water depth h to the wavelength λ is large. For practical applications, a deep-water condition is already satisfied when $h/\lambda > 1/2$. Finally, we are interested in configurations in which dissipation is negligible and consequently do not consider viscous effects of any kind: solid boundaries, wave breaking, etc.

This classical set of assumptions for water waves leads to the modeling of this physical phenomenon due to the nonlinear potential flow theory. This has been widely used to study several nonlinear wave phenomena such as nonlinear wave interactions [9], RWs [28,29], and water-wave turbulence [30]. Numerical solutions of the fully nonlinear problem can be complex and very time consuming from a numerical point of view. An alternative to overcome these constraints is to assume weak nonlinearity of the wave field, while processes are expected to be narrow banded, allowing slow modulations. With these additional hypotheses, one may use the focusing NLSE [9] to describe the evolution of nonlinear narrow-banded wave trains in deep water

$$i\left(\frac{\partial\psi}{\partial t}+\frac{\omega}{2k}\frac{\partial\psi}{\partial x}\right)-\frac{\omega}{8k^2}\frac{\partial^2\psi}{\partial x^2}-\frac{\omega k^2}{2}|\psi|^2\psi=0, \tag{1}$$

while $\psi(x,t)$ is the complex envelope of the corresponding wave train. To the second-order of approximation in wave steepness ka ($k=2\pi/\lambda$ is the wave number and a stands for the wave amplitude), the free surface elevation is then given by

$$\eta(x,t)=\mathrm{Re}\left\{\psi(x,t)\exp[i(kx-\omega t)]+\frac{k\psi^2(x,t)}{2}\exp[2i(kx-\omega t)]\right\}. \tag{2}$$

In the following we consider exact analytic solutions to the NLSE to assess the validity of the TR procedure. The simplest form is the stationary envelope solution [31]. The most prominent form of breathers is the family of doubly localized breathers, also referred to as Akhmediev-Peregrine breathers [32,33], which have been emphasized to be appropriate models to describe oceanic RWs [34,35]. A detailed description and parametrization of those analytic solutions are given in the Supplemental Material [36].

For a given solution $\psi(x,t)$ of Eq. (1), it can be easily verified that the time-reversed complex conjugate form $\psi^*(x,-t)$ is also a solution. Therefore, both corresponding free surface elevations $\eta(x,t)$ and $\eta(x,-t)$ are possible solutions to the water-wave problem within the framework of the NLSE. Due to this property, a TR mirror can be used to create the time-reversed hydrodynamic wave field $\eta(x,t)$ in the whole propagating medium.

The theory indicates that to be effective, the TR procedure needs to measure and time-reverse the free surface elevation as well as the normal velocity of this surface. However, from a practical point of view, in water waves experiments, no simple generation procedure exists to ensure both those quantities at the same time. We consequently restrict our study to practical applications in laboratories (for instance, ocean engineering facilities) in which the only free surface elevation is imposed or controlled by a wave maker. Indeed, it has been shown experimentally [21,23] that this procedure is efficient. If the problem has only one horizontal spatial dimension, it appears sufficient to measure the wave field at one location $\eta(x_M,t)$ and rebroadcast the time-reversed signal $\eta(x_M,-t)$ from this unique point x_M (mirror position) in order to observe the solution $\eta(x,-t)$ in the whole medium and thus to verify the TR invariance.

Within a water-wave basin, the possible procedure to verify the validity of the TR procedure is to (i) generate a given wave field, (ii) measure the spreading waves at a specific location, and (iii) time-reverse this signal and use it to generate a new wave field. If time-reversibility is valid, the wave field measured by the probe, during the second experiment, should correspond to the pulse generated by the wave maker's motion of the first experiment.

Time-reversal has been experimentally studied in a wave basin within the framework of breathers in Ref. [23] for initial solutions that exhibit strongly nonlinear features. In fact, doubly localized breathers up to second-order have been accurately refocused through time-reversal. This indicates that the TR procedure, in the presence of high nonlinearity and dispersive effects, is still valid. It allows the use of the time-reversible feature of the wave field, even in the case of strong focusing.

The purpose of the proposed study is to detail the range of applicability of the TR method for water waves in the configuration of a unidirectional wave basin. As stated previously, the time-reversibility can be demonstrated in the context of the NLSE and is also theoretically valid for the fully nonlinear conservative water-wave problem (potential flow formalism). However, the practical TR procedure relies on some assumptions that may result in a loss of accurate wave refocusing (use of the only free surface elevation, conversion to the wave maker's motion, etc.). We will show that the application of the TR procedure to NLSE solutions is indeed valid for a significant range of parameters. Therefore, even if the target wave field is only an approximation to the fully nonlinear physics of the water-wave problem (assuming weak nonlinearity and narrow-banded dynamics), the TR procedure is applicable. In this regard, the important parameters for this study are expected to be

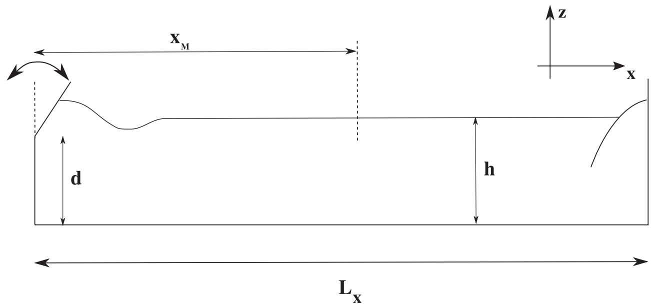

FIG. 1. Sketch of the NWT.

(i) nonlinearity, characterized by the steepness of the wave field ka, and (ii) higher-order dispersive terms, appearing to be non-negligible, when the process is broad banded. The latter effects related to higher-order dispersion can be characterized through the propagating distance kx_M.

III. NUMERICAL WAVE TANK CONFIGURATION AND GENERATION OF HYDRODYNAMIC LOCALIZED STRUCTURES

Following the experiments presented in Ref. [23], a numerical procedure is set to provide an extensive analysis with respect to the applicability and limitations, related to the use of the TR approach for nonlinear waves in a wave basin. This section presents the numerical model as well as the setup validation.

A. Numerical wave tank

The numerical validation of the TR procedure in the context of water waves relies on an accurate description of the wave physics at play during the wave propagation. Primarily, it has been discussed in the previous section that possible limitations are due to high-order nonlinearities and high-order dispersive terms. Consequently, the suitable numerical model must include these physical features in the configuration of the nonlinear potential flow solver, being the typical candidate, if we exclude the breaking of the waves.

The HOS model [25,26], described briefly in the Supplemental Material [36], has been widely used in the context of water waves for the study of specific nonlinear processes such as modulation instability [16,37], simulation of RWs in irregular sea states [28], or emergence of bimodal seas [38]. This highly nonlinear scheme allows an efficient and accurate solution of the water-wave problem.

This original HOS model is however limited to the study of nonlinear waves propagating in a periodic domain, specifying an initial condition. The configuration is essentially different in the context of a wave basin. This exhibits a wave maker to generate a given wave field, an absorbing beach on the other side of the basin to prevent wave reflections as well as reflection conditions on the sidewalls. Consequently, specific attention has been paid to the development of a NWT that includes all those specificities, which we refer to as a HOS NWT. This model has been validated with several comparisons to experiments on different wave fields: from regular unidirectional waves to directional irregular sea states (see [24] for details).

In the following, the configuration used for the NWT is similar to the experiments reported in Ref. [23]. The unidirectional wave field will be analyzed in the configuration, sketched in Fig. 1 for the sake of appropriate analysis dimensions. The wave maker is defined as a hinged flap and the numerical absorbing beach is designed so that no reflection occurs during the simulations. The water depth is defined as $h = 1$ m, the hinged location is $d = 0.8$ m, and the length of the basin is set to be $L_x = 20$ m.

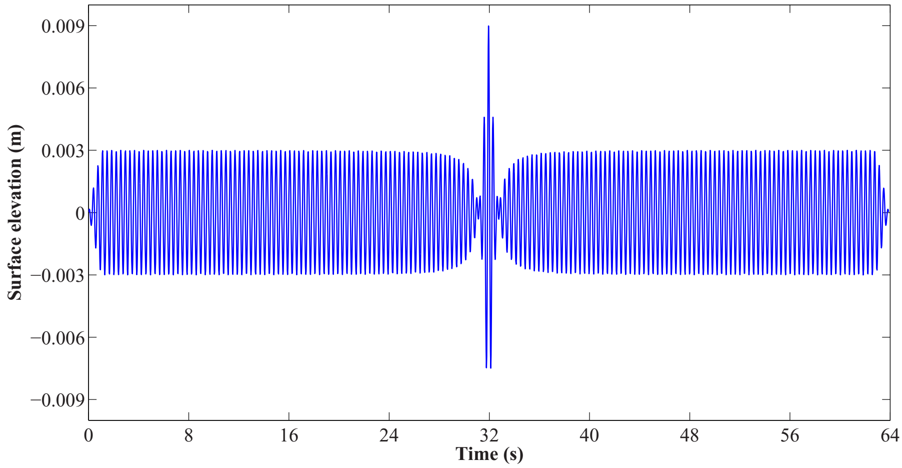

FIG. 2. Target wave elevation used to define the wave maker's motion: Peregrine breather with $ka = 0.09$ and $a = 0.003$ m, evaluated at $x = 0$.

The numerical parameters in the HOS NWT have been chosen to ensure an accurate description of the physical phenomena at stake. These are detailed in the Supplemental Material [36].

B. Generation of a localized wave field

We start the TR procedure by first defining the temporal surface wave profile of the pulse to be studied $\eta(x_S,t)$ at the source (wave maker) position x_S. As specified earlier, different specific NLSE pulses for several wave parameters will be investigated in this work. The choice of the analytic envelope soliton, or doubly localized structures, will define the complex envelope $\psi(x,t)$ and the corresponding target free surface elevation at the maximal envelope amplitude $\eta(x = 0,t)$ through Eq. (2). This allows us to define the wave maker's motion through the use of an adequate transfer function, dependent of the wave maker's shape. The TR procedure consequently relies on a linear approximation to relate the target free surface elevation to this motion, leading to possible discrepancies.

We demonstrate the procedure by means of the Peregrine solution. Figure 2 gives an example of the free surface profile $\eta(x = 0,t)$ used to deduce the wave maker's motion. This is the case of a Peregrine breather with carrier wave steepness $ka = 0.09$ and a carrier amplitude $a = 0.003$ m, evaluated at $x = 0$. We used ramps at the beginning and end of the chosen time window in order to ensure (i) a smooth start of the wave maker's movement and (ii) the periodicity of the signal, which is decomposed on Fourier components.

In the different configurations tested, the time window of the target free surface elevation is kept constant and is specified and depicted in Fig. 2. This corresponds to $T_w \simeq 175T_0$, with $T_0 = 2\pi/\omega$ the carrier wave period. This is sufficiently long to prevent from any boundary effects on a sufficiently long time window around the modulation, which occurs around $\simeq 110T_0$, as presented in Ref. [23].

Once the first wave field is recorded at the specified probe mirror location x_M, we time-reverse this signal and use it as a novel wave maker's signal (still using the same linear transfer function) for the follow-up TR refocusing experiment. Figure 3 presents an example of the recorded signal in the case of the Peregrine breather as well as the corresponding time-reversed time series, injected into the wave maker for $ka = 0.09$ and $kx_M = 270$. Note that the time origin has been shifted to take into account the propagating distance ($t' = t - x_M/C_g$).

Finally, due to the spatial reciprocity, the time-reversed and second wave field is generated at the same source and recorded at the same mirror location x_M. This allows us to compare the focused wave profile to the original signal, as shown in Fig. 4. Details about the comparisons and validations

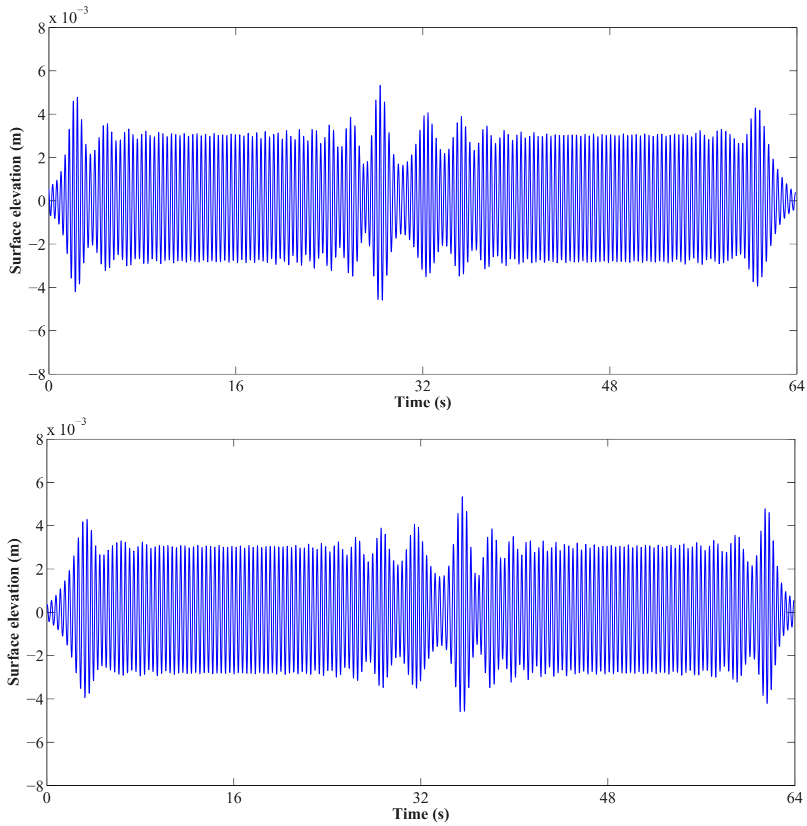

FIG. 3. Peregrine breather surface elevation with $ka = 0.09$ and $a = 0.003$ m. Shown on top is the probe signal measured at x_M after the propagation on a distance $kx_M = 270$ and on the bottom is the time-reversed signal, providing a new wave maker's boundary condition.

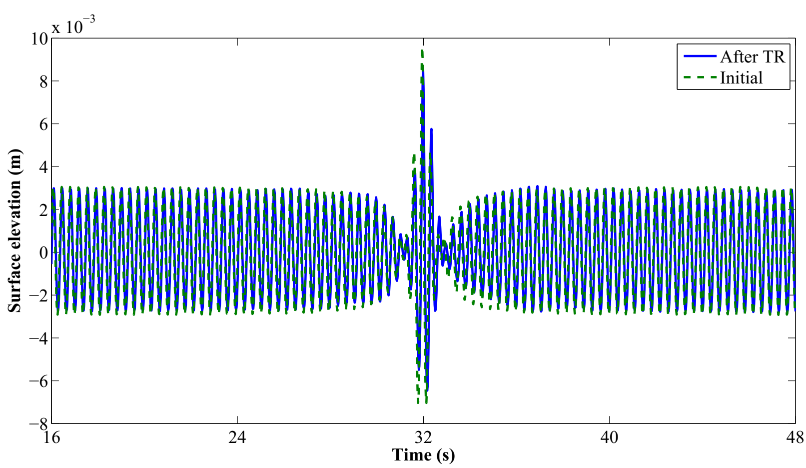

FIG. 4. Comparison of the Peregrine surface profile as generated by the wave maker (dashed line) with the reconstructed and refocused waves after the TR procedure (solid line). The carrier parameters are $ka = 0.09$ and $a = 0.003$ m, while $kx_M = 270$.

with respect to the results presented in Ref. [23] are provided in the Supplemental Material [36]. The case of the doubly localized Peregrine breather and the second-order Akhmediev-Peregrine breather are validated. It shows that the proposed numerical procedure, based on the use on the highly nonlinear HOS NWT, provides an accurate description of the complex physics involved in the wave generation and propagation. The next step is now to make use of the proposed procedure to study the application range of the time-reversal in the context of water waves with respect to the steepness (nonlinearity) and the propagation distance (dispersion) for an accurate TR refocusing.

IV. VALIDITY OF THE TIME-REVERSAL APPROACH

Realistic sea state conditions may exhibit configurations in which nonlinearities may become significant [39]. Taking into account this fact as well as the chaotic nature of ocean waves, it is consequently interesting to study the possible limitations to the use of time-reversal for those wave conditions. This would allow us to determine the limitations in tracing back oceanic extreme events.

In this study we reduce our attention to simple stationary and highly nonlinear pulsating states, as determined by the NLSE. The parameters studied are reduced to the wave steepness ka, which characterizes the nonlinearity of the wave field, as well as the maximal propagation distance required for an accurate TR refocusing kx_M, which characterizes the effects of dispersion. As simple artificial sea state configurations, we consider the stationary envelope soliton solution, followed by the two doubly localized breathers of first and second-order, respectively.

It appears necessary to use an accuracy estimator to evaluate the validity of the TR technique. This is based on the free surface elevation recorded by the wave gauge after application of time-reversal, namely, $\eta_{TR}(t)$. In the context of the reproduction of extreme waves in wave basins, it has been shown in Ref. [40] that the most important parameter to ensure the correct kinematics inside the fluid domain, also essential, for example, to study wave-structure interactions, is the wave amplitude. Consequently, the chosen accuracy parameter is defined by

$$R_{\text{amp}} = \frac{\max(\eta_{\text{TR}})}{\max(\eta_{\text{NLSE}})}, \tag{3}$$

while η_{NLSE} denotes the analytic free surface elevation obtained from the NLSE (2). This expression includes the second-order bound waves whose contribution becomes more distinct when strong localized focusing in the wave train emerges. This parameter appears appropriate to have an accurate estimation of the quality of the TR refocusing. As we will see in the following, discrepancies will be characterized by a possible change of shape or time shifts. Nevertheless, these discrepancies have been always associated with a change of amplitude that is relevant as an indicator of global accuracy.

Note that the maximum steepness, chosen in the different test models presented, is below breaking-steepness thresholds, related to each solution considered. Indeed, choosing large steepness values for the carrier, modeled by breathers in particular, may engender breaking, making these wave trains unsuitable for accurate studies within the context of the NLSE and for the HOS NWT based simulations. We therefore limit this study to the range of stability of experiments and numerical computations.

A. Stationary envelope solitons

We present here the application of the TR refocusing approach to the case of envelope solitons, varying the initial steepness ka and dimensionless propagating distance kx_M accordingly. Figure 5 presents the accuracy estimator R_{amp} as a function of these two parameters.

First, it is obvious that the accuracy of the TR method is indeed dependent on the two parameters of interest in this study, allowing the quantification of nonlinearities and dispersive properties of the considered wave field. We observe that increased nonlinearity of the wave field leads to a less accurate reproduction of the target wave field. These high-order effects start to be very important from $ka \simeq 0.20$ and have a significant influence on the quality of the procedure above this value.

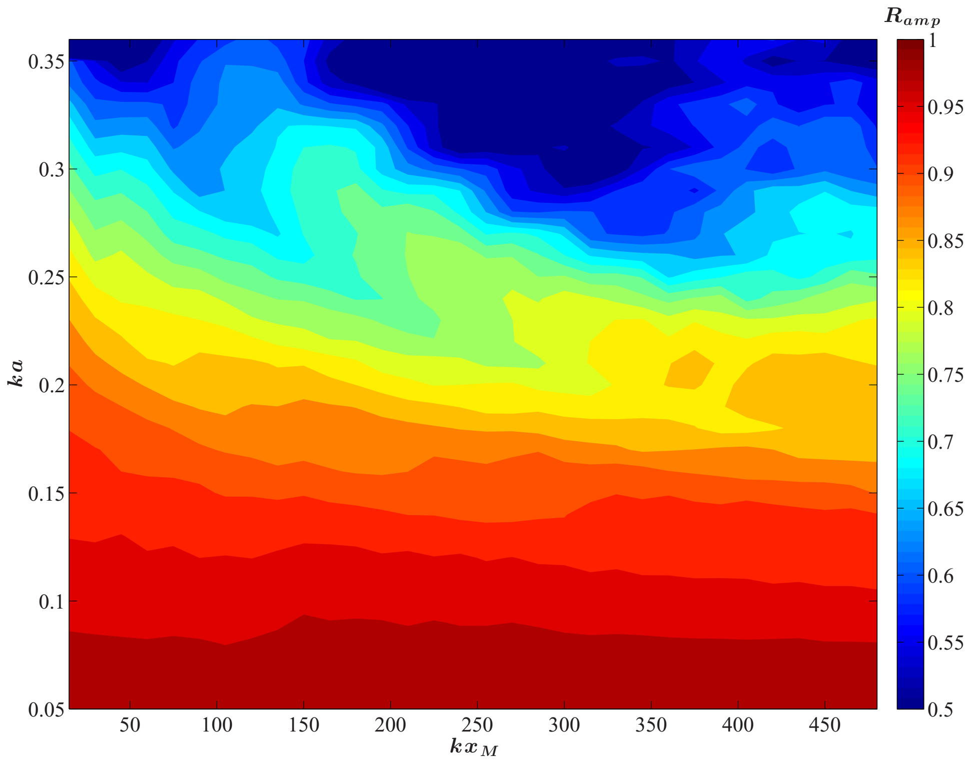

FIG. 5. Accuracy diagram of the time-reversal for the stationary envelope soliton R_{amp} as a function of initial steepness ka and propagating distance kx_M.

Furthermore, the correlation amplitude factor R_{amp} of the considered sech-wave pattern starts to drastically reduce when approaching the wave-breaking limit. Note that experimental results dealing with the one-way propagation of such a wave field (no TR procedure), reported in Ref. [41], show that at a steepness of $ka = 0.35$ strong distortions of the NLSE envelope soliton are noticed.

At the same time, also clearly noticeable is that larger propagating distances also decrease the accuracy of the TR procedure accuracy. The propagating distances studied here range from $kx_M = 15$ up to $kx_M = 480$, representing indeed significant long evolution distances. High-order dispersive and nonlinear effects may consequently have indeed an influence on the TR procedure (i.e., generation, propagation, and measurement of the wave field followed by the refocusing), breaking down the time-reversibility in the proposed configuration.

In order to refine the analysis of the origin of the discrepancies observed between initial and reconstructed free surface elevations, we present the simulation results, obtained for the steepness $ka = 0.30$, an amplitude of $a = 0.01$ m, and the propagating distance $kx_M = 330$. The corresponding amplitude ratio in this case is $R_{\text{amp}} = 0.54$, indicating low accuracy of the TR procedure with this choice of parameter. Figure 6 shows the corresponding results after the first propagation in the NWT.

We can observe that the initial envelope soliton starts to disintegrate during its propagation and its dynamics is not in agreement with NLSE predictions. Again, this is in agreement with [41]. The initial sech-shaped solution starts to fission into smaller-amplitude solitons [42]. Figure 7 depicts the comparison of the initial envelope soliton and the free surface elevation, reconstructed through time-reversal.

We notice that neither the initial amplitude nor the initial location could be reconstructed. The initial deterioration of the envelope after the first propagation is exacerbated by the time-reversal after the second evolution. This means that from the first wave measurement (Fig. 6), the TR procedure

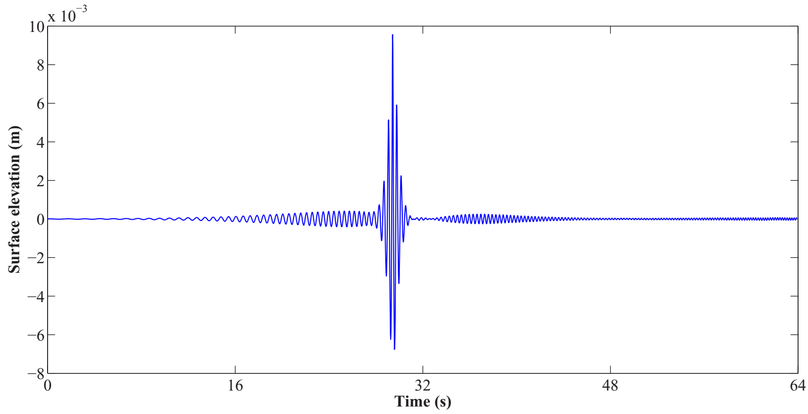

FIG. 6. Free surface elevation of the envelope soliton for an amplitude $a = 0.01$ m with a steepness of $ka = 0.30$, recorded at the probe after a dimensionless propagation distance of $kx_M = 330$.

that deduces a new wave maker's signal and a second propagation induces some discrepancies that break down the time-reversibility. In fact, significant higher-order effects in terms of nonlinearities and dispersion are thus associated with the reduced accuracy. Those features will be studied in more detail with the analysis of doubly localized breathers.

B. Doubly localized breathers

The study of limitations of the TR approach for breathers is obviously more challenging than the previous stationary case. The first- and second-order doubly localized breathers have the property of an infinite modulation period, exhibiting a strong variation of the wave envelope and therefore of the spectra as well. Detecting the limitations of applicability of the TR procedure may be transferred to assigning limitations with respect to the reconstruction of an extreme event in the ocean within the framework of integrable evolution equations.

As mentioned earlier, the accuracy of the NLSE and applicability of the TR technique are closely linked to the initial steepness ka of the carrier. A similar dependence on the propagating distance kx_M can be also expected.

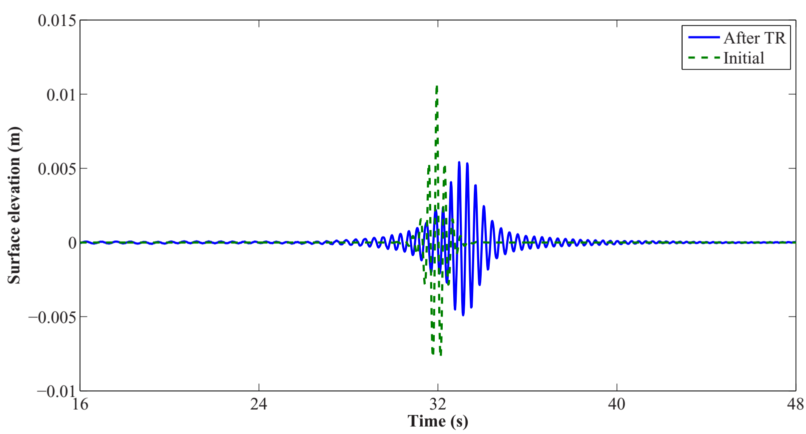

FIG. 7. Results of time-reversal for an envelope soliton for an amplitude $a = 0.01$ m, steepness $ka = 0.30$, and $kx_M = 330$.

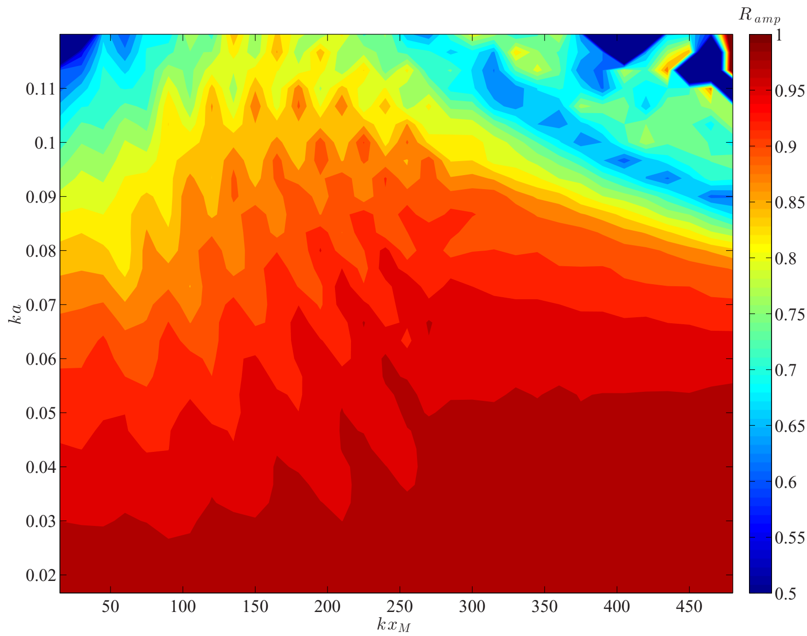

FIG. 8. Accuracy diagram of the time-reversal for the doubly localized Peregrine breather R_{amp} as a function of initial steepness ka and propagating distance kx_M.

1. Peregrine breather

We propose here some complements to Fig. 4, which depicts a result of the TR method for a given steepness $ka = 0.09$ and propagating distance $kx_M = 270$ in the case of a Peregrine breather. Figure 8 presents the accuracy of the refocusing after the time-reversal in terms of the amplitude of the extreme wave R_{amp}. The parameters of interest are varied in a range $kx_M \in [15{,}480]$ and $ka \in [0.02{,}0.12]$. Recalling that the theoretical amplification of the plane wave for a Peregrine breather is 3, this choice of steepnesses covers the whole range of existence of such localized structures, below the breaking threshold, experimentally determined as being at a steepness value of about 0.12 [43].

It is also confirmed in this case that the accuracy of the approach is improved when the steepness is lower. In fact, we can ensure an accurate validity of TR refocusing for the whole range of dimensionless distance kx_M, for steepness values below $ka < 0.075$. Here we also emphasize a slight decrease of accuracy in the latter range for small propagation distances $kx_M < 100$–150.

Note that Fig. 8 allows us to extract the accuracy of laboratory breather TR experiments, as described in Ref. [23]. Indeed, for the chosen propagating distance $kx_M = 270$ the time-reversal for the Peregrine breather with good exactitude applies up to a steepness $ka \simeq 0.09$ (consistent with the successful experiments in Ref. [23] conducted for $ka = 0.09$). We recall that the local steepness of the largest wave in the group is indeed very large and can be roughly estimated as being three times the carrier steepness, which is approximately $3ka \simeq 0.27$. Taking into account the theoretical limitations of the practical TR procedure, as well as the laboratory or numerical noise, always present in the experiment, the validity of the TR approach for this range of parameters is remarkable.

As stated previously, beyond $ka > 0.075$, a good accuracy of TR refocusing can still be noticed for some values of steepness and dimensionless propagation distance. However, this validity range is not as obvious. This will be studied in more detail in Sec. V.

2. *Akhmediev-Peregrine breather*

In the case of a second-order doubly localized breather, validations of the TR refocusing are provided in the Supplemental Material [36] for $ka = 0.03$ and $kx_M = 270$. Figure 8 extends this study and presents a more general accuracy diagram with respect to the parameter R_{amp} as a function of initial steepness ka and propagating distance kx_M, as in the previous case. The range of parameters is $kx_M \in [15,480]$ and $ka \in [0.01,0.072]$. We have to recall that for this specific solution, the theoretical amplification of the plane wave is 5. Again, the range of steepness values has been chosen to prevent breaking of the highest amplified waves.

The dependence of R_{amp} on to the two parameters is very similar to the case of the Peregrine breather. That is to say, the accuracy of the TR approach is reduced when the steepness is increased. At the same time, the accuracy is also reduced at large propagating distances and slightly altered for $kx_M < 100$–150. Figure 8 may be used to show that for the whole range of propagating distances studied, the TR method allows correct refocusing up to $ka \simeq 0.045$. For the same example as in the previous section (i.e., $kx_M = 270$), the TR method allows correct refocusing up to $ka \simeq 0.055$, which is at a local steepness in the modulation $5ka \simeq 0.28$.

As a general conclusion of the previous test cases, it has been shown that the TR method is efficient for a large range of steepnesses and propagating distances. Different kinds of wave envelope patterns have demonstrated a similar behavior. However, the practical setup of time-reversibility of water waves fails for large steepness or very large propagating distances. The TR procedure will allow an accurate refocusing when the local steepness of the localized structures do not exceed a general value of about $ka \simeq 0.25$. Nevertheless, we are optimistic about possible applications of time-reversal for ocean waves, considering the fact that ocean waves have the property of reduced steepness values most of the time. More physical insights with respect to the TR approach will be provided in the next section.

V. PHYSICAL INTERPRETATION OF THE HOS NWT SIMULATIONS

This section is devoted to the analysis of the limitations of the TR method, as reported in the previous section. For the sake of brevity, we focus on one particular case, namely, the Peregrine breather for the steepness parameter $ka = 0.09$, propagating forth and back for $kx_M = 270$. We provide a rigorous analysis of the possible influence of the propagating distance and then of the steepness. Note that essentially similar results are obtained in the case of the Akhmediev-Peregrine breather.

A. Influence of propagating distance kx_M

As explained previously, one source of discrepancies is associated with the practical setup of the TR procedure in the context of water waves. The wave maker imposes the only free surface elevation and is deduced from linear theory. This will influence the way the breather will propagate and consequently we expect the effects to become increasingly significant with the increase of the propagating distance. This is the probable origin of the behavior observed in Figs. 8 and 9 at large distances of evolution.

Note that the time scale of Benjamin-Feir (BF) instability is determined by $t_{\mathrm{BF}} = O(T_0/(ka)^2)$. The corresponding length scale of this modulation instability is $kx_{\mathrm{BF}} = kC_g t_{BF} = O(1/(ka)^2)$, with C_g the group velocity. It is known that this BF instability is at the origin of the possible existence of localized structures such as breathers [11]. In the present case $1/(ka)^2 \simeq 125$ and consequently the propagating distances studied are in the range of the scale of the modulation instability processes. This also indicates that there is indeed a strong link between the propagating distance kx_M and the steepness of the considered wave field ka. As a complement, Fig. 10 presents for the previous accuracy diagram isolines corresponding to this BF instability in the range $kx_{\mathrm{BF}} \in [1,2]$.

This instability appears consequently as a major point in the understanding of the limitations inherent to the TR method. In the case of a Peregrine breather, when the propagating distance is

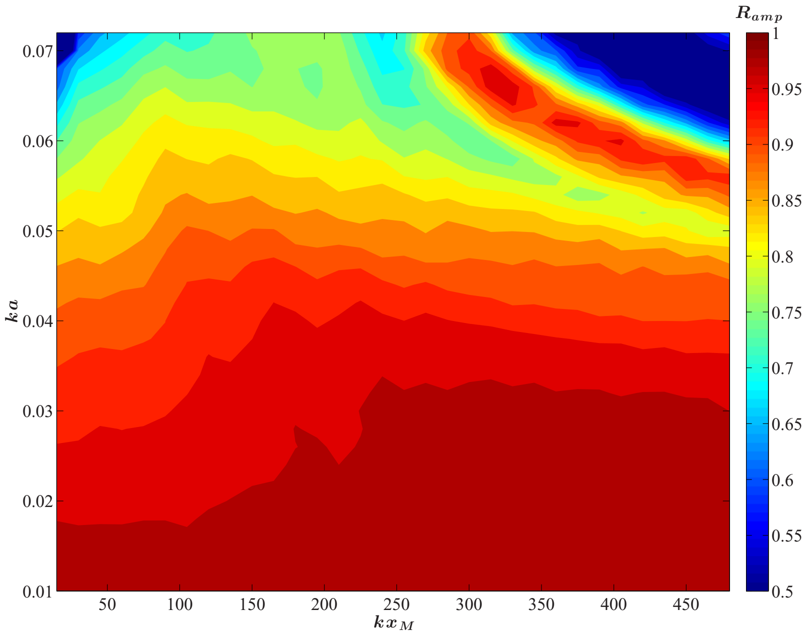

FIG. 9. Accuracy diagram of the time-reversal for the doubly localized Akhmediev-Peregrine breather of order two R_{amp} as a function of initial steepness ka and propagating distance kx_M.

larger than about 1.8 times the length scale of BF instability, the applicability of the TR method starts to fade. This can be related to the scale of evolution of the breather solution to NLSE and the development of the possible perturbations to this solution.

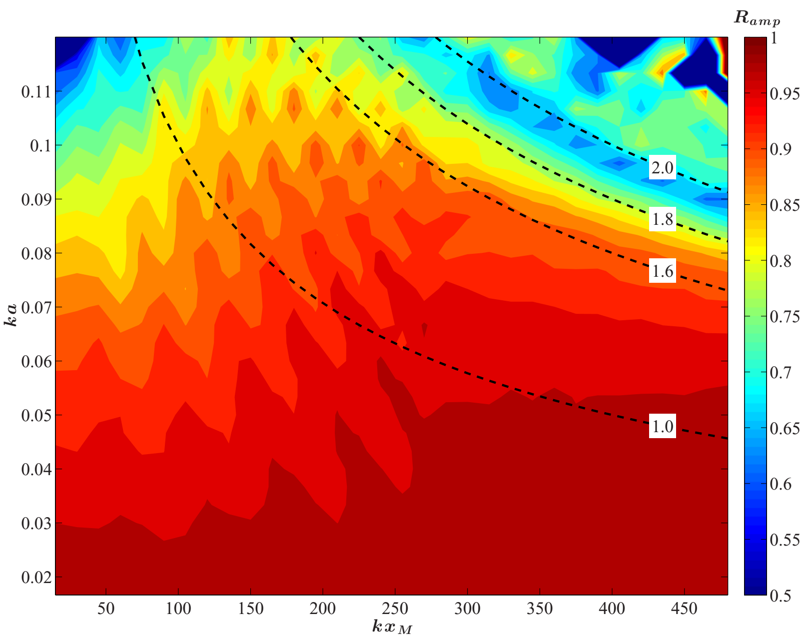

FIG. 10. Accuracy of the TR method for the Peregrine breather. Dashed lines are isolines in terms of the modulation instability process.

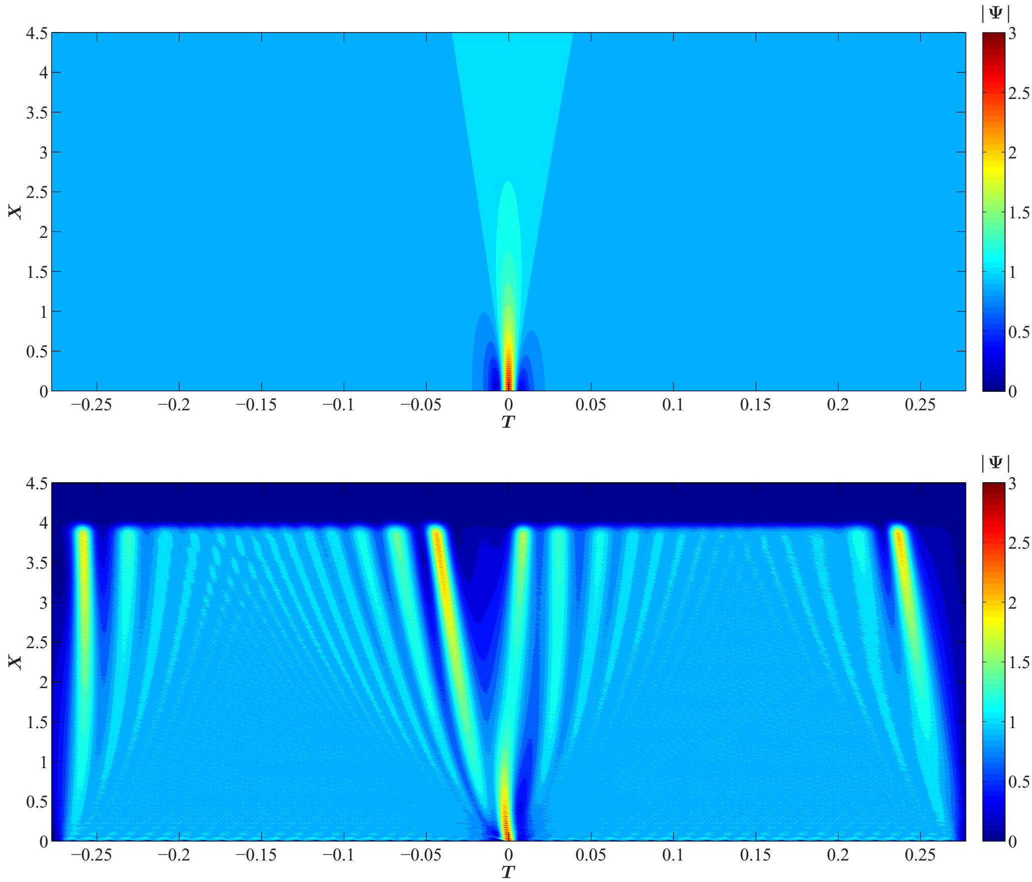

FIG. 11. Propagation of the Peregrine breather ($ka = 0.09$) in the wave basin, space-time representation in scaled NLSE variables: comparison of the analytic solution (top) and the HOS NWT numerical simulation (bottom).

In addition to the free surface time signals, numerical simulations enable a general overview of the wave field evolution. Figure 11 presents a full space-time depiction of the propagation inside the wave basin. The variables are changed to NLSE scaled variables $X = \sqrt{2}k^2ax$ and $T = -\frac{k^2a^2\omega}{4}(t - x/C_g)$ for comparison to the analytic solution. We recall that an absorbing zone is present to prevent wave reflections on the end wall in the HOS NWT simulations. This appears clearly in Fig. 11 at $X > 4$.

The demodulation of the initial localized structure with respect to the propagating distance is obvious during its evolution. However, it is also worth noting that the solution does not tend to the plane-wave solution after a long-time and long-distance propagation for this choice of carrier parameters, as expected from NLSE theory. Note that it has been verified that this is not related to the finite extent in time of the generated wave train.

At the same time, an asymmetry of the temporal wave probe signal can also be observed after the first propagation. Indeed, the NLSE predicts a symmetric demodulation with respect to time, at a fixed spatial location, which appears to be erroneous when nonlinearities are important. This fact is well known and has already been pointed out in different studies. It has been shown that the higher-order NLSE, also referred to as the Dysthe equation, enables a nonsymmetric prediction of the envelope evolution [16,44–47] when the steepness of the carrier and the amplitude amplification become substantial.

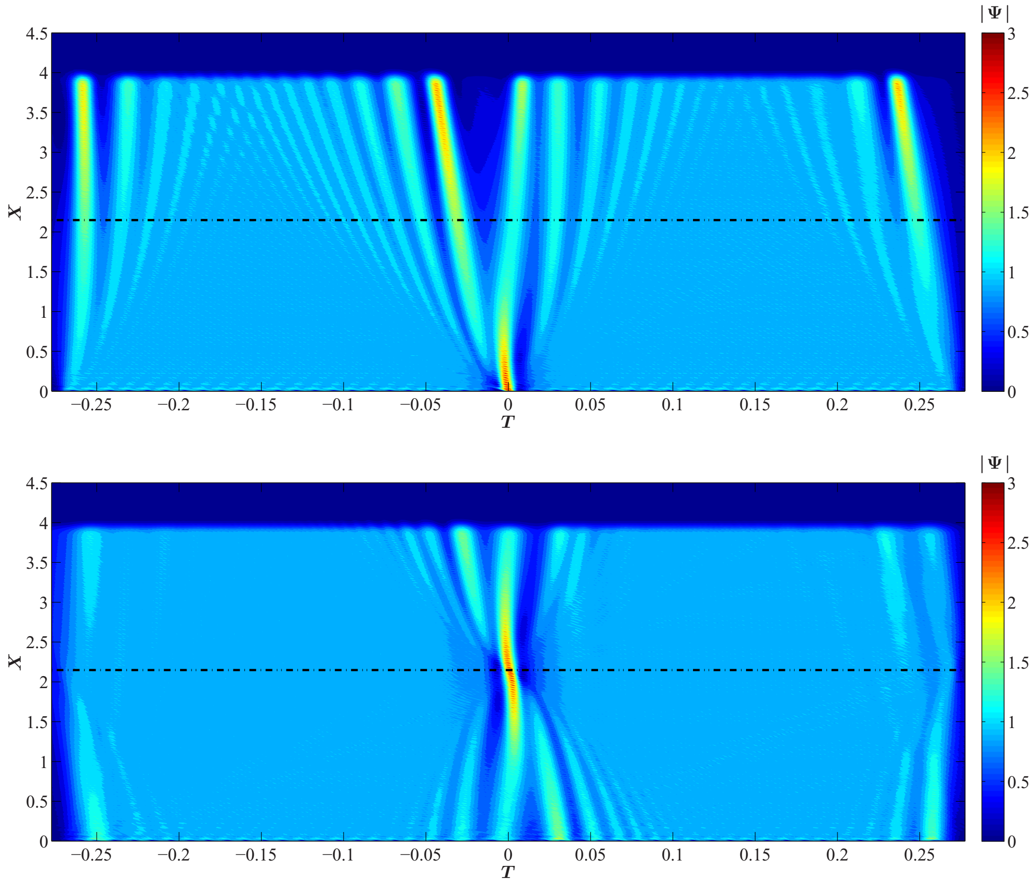

FIG. 12. Space and time evolution of the Peregrine breather for $ka = 0.09$ and $kx_M = 270$ (dash-dotted line) in the NWT: demodulation (top) and TR refocusing (bottom).

Nevertheless, as shown previously in Fig. 4, the observed and expected asymmetry does not influence the TR invariance. Figure 12 depicts the space and time evolution of the Peregrine wave field during the first propagation and for the TR wave refocusing. The case of the Peregrine breather for $ka = 0.09$ and the propagating distance of $kx_M = 270$ is adopted here. This corresponds to a scaled distance $X_M \simeq 2.1$ depicted in the figure.

The time-reversibility is clearly demonstrated during the whole HOS NWT computation, throughout the whole spatial domain. Again, this confirms the accurate refocusing presented in Fig. 4 and in the experiments in Ref. [23]. This point is of major importance since even if the wave field evolution clearly departs from the NLSE prediction, the full nonlinear system appears as time-reversible. The TR procedure enables the use of such a property of the wave field, even in the case of high nonlinearity.

The influence of the propagating distance is now studied on the previous test cases by gradually increasing the values of kx_M. Figure 13 shows the final refocusing results of the complete TR procedure for $kx_M \in \{60,165,270,375,480\}$ at a fixed steepness of $ka = 0.09$.

We can observe in Fig. 13 that the influence of the propagating distance on the reconstruction is quite complex. For relative small propagating distances ($kx_M < 100$), the global shape of the localized structure is correct but is associated with a reduced amplitude at the location of the extreme wave. Then, for a significant range $kx_M \in [100,350]$, the TR procedure is very accurate in the refocusing of the localized structure of interest. The influence of the propagating distance is then to

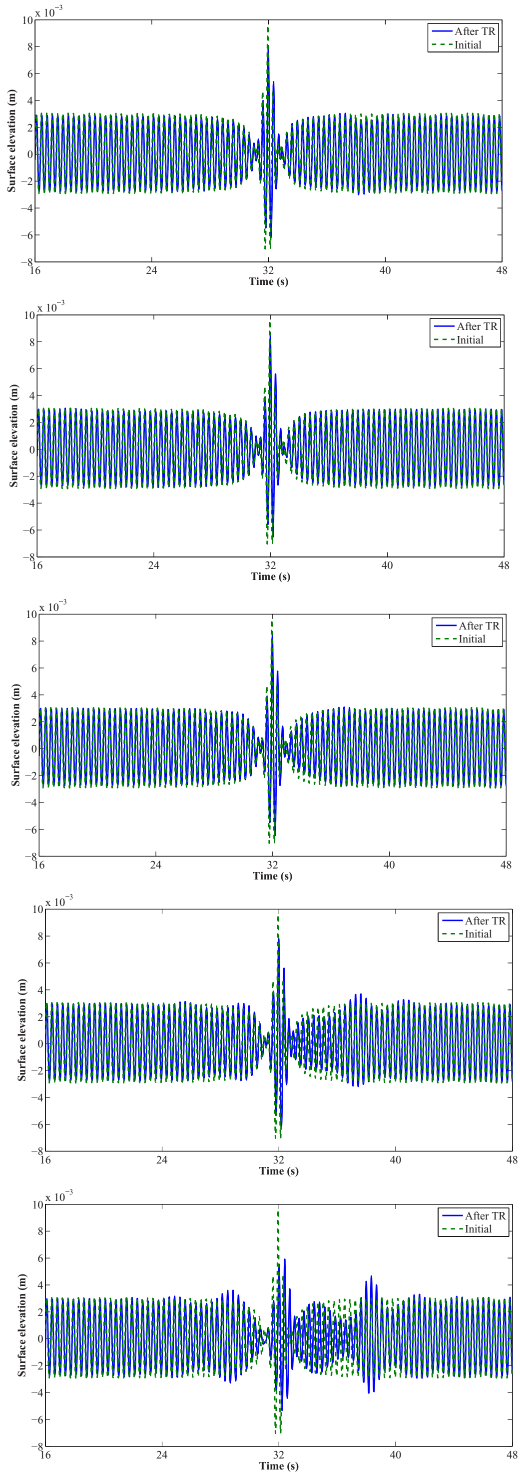

FIG. 13. Comparison of the Peregrine surface profile at maximal compression, as initially generated with respect to the NLSE theory (dashed line) and after TR refocusing (solid line), for $ka = 0.09$ and $kx_M \in \{60, 165, 270, 375, 480\}$ (from top to bottom).

induce an increasing but still very small phase shift between the refocused solution and the original one. Finally, for very large evolution distances, starting from $kx_M \simeq 375$, the slight phase shift after time-reversal is associated with an ineffective refocusing. This leads to a complex wave field distortion and wave profile that significantly deviate from the initial doubly localized structure. As can be seen in Fig. 13, the effect is more pronounced when the distance is enlarged.

Also, the origin of this distortion is not straightforward to explain. It is recalled here that two processes of wave generation and propagation have to be successively conducted in order to obtain the final TR result.

The first generation associated with the propagation creates a nonlinear wave field (which can be different from the NLSE solution due to high-order effects and/or discrepancies of the wave maker's motion). Then, during the second stage of TR refocusing, some information may be lost when deducing the new wave maker's motion from the measured free surface elevation $\eta(x_M, t)$ (recall that we use linear theory for this purpose). Consequently, the final phase shift or change of observed envelope shape is a kind of footprint with respect to the existence of nonreversible effects in the TR procedure. These are related to nonlinearities possibly with dispersive effects.

The first influence of the propagation distance is the increase of the phase shift after the use of the TR method. This reduces the accuracy of the refocusing at large distances. Then those effects are obviously more enhanced at even larger propagation distances and lead to the failure of the TR procedure. As stated previously, we can evaluate that the length scale of this limitation of applicability is associated with the modulation instability space scale.

Finally, we would like to address the unexpected validity of the TR approach in all temporal signals at smaller propagating distances ($kx_M < 150$), as can be observed in Fig. 8. It is known that during the generation of waves by a wave maker, the so-called evanescent waves are spontaneously created when the wave field is generated. These waves are only relevant close to the wave generator since they quickly decay in space. In the configuration tested, they are therefore negligible considering the whole range of propagation distances for $kx_M \geqslant 15$. In addition, parasitic second-order free waves are also generated with the target wave field [48]. As a first approximation, if we consider the waves to be regular, this parasitic wave field consists of regular free waves with a pulsation $\omega_2 = 2\omega$. Those waves will propagate at a velocity that is half the velocity of the corresponding waves we are interested in generating and reach the probe position of interest at $t_2 = 2x_M/C_g$. We recall that figures presenting probe signals are already time shifted with $t_{\text{shift}} = x_M/C_g$. In this time reference frame, the parasitic second-order free waves, generated by the wave maker, will reach the probe at a time $t_2' = x_M/C_g$. For the case $kx_M = 60$ presented in Fig. 13, this corresponds to $t_2' \simeq 7$ s. It can be seen on the free surface wave profile that after the breather with a delay t_2', unexpected discrepancies are present that are associated with the parasitic second-order waves.

Thus, these waves are at the origin of the reduced accuracy at relatively small propagating distances $kx_M < [100,150]$ as reported in Fig. 8. Indeed, in this range of distance, the parasitic free waves are recorded after the first propagation for the corresponding propagating time is $t_2' < [12,17]$ s. Consequently, during the refocusing of the waves, these are generated again and interfere with the localized structure, reducing the corresponding accuracy as a consequence. It should be noted that it is possible to control the generation of the parasitic waves, produced by the wave maker as explained in Ref. [48]. The wave maker's motion can then be modified in order to prevent the generation of those waves. This approach may be used to possibly increase the accuracy of the TR method.

B. Influence of initial steepness ka

This section focuses on the influence of the nonlinearity on the TR procedure. As observed previously, the Peregrine solution imposed at the wave maker's location does not tend to the plane-wave solution after a long-time and long-distance propagation, as expected from the NLSE, for significant carrier steepness values.

The previous section presented the influence of the propagation distance kx_M on a TR refocusing accuracy at a fixed steepness ka. We will now fix the mirror location and vary the steepness values

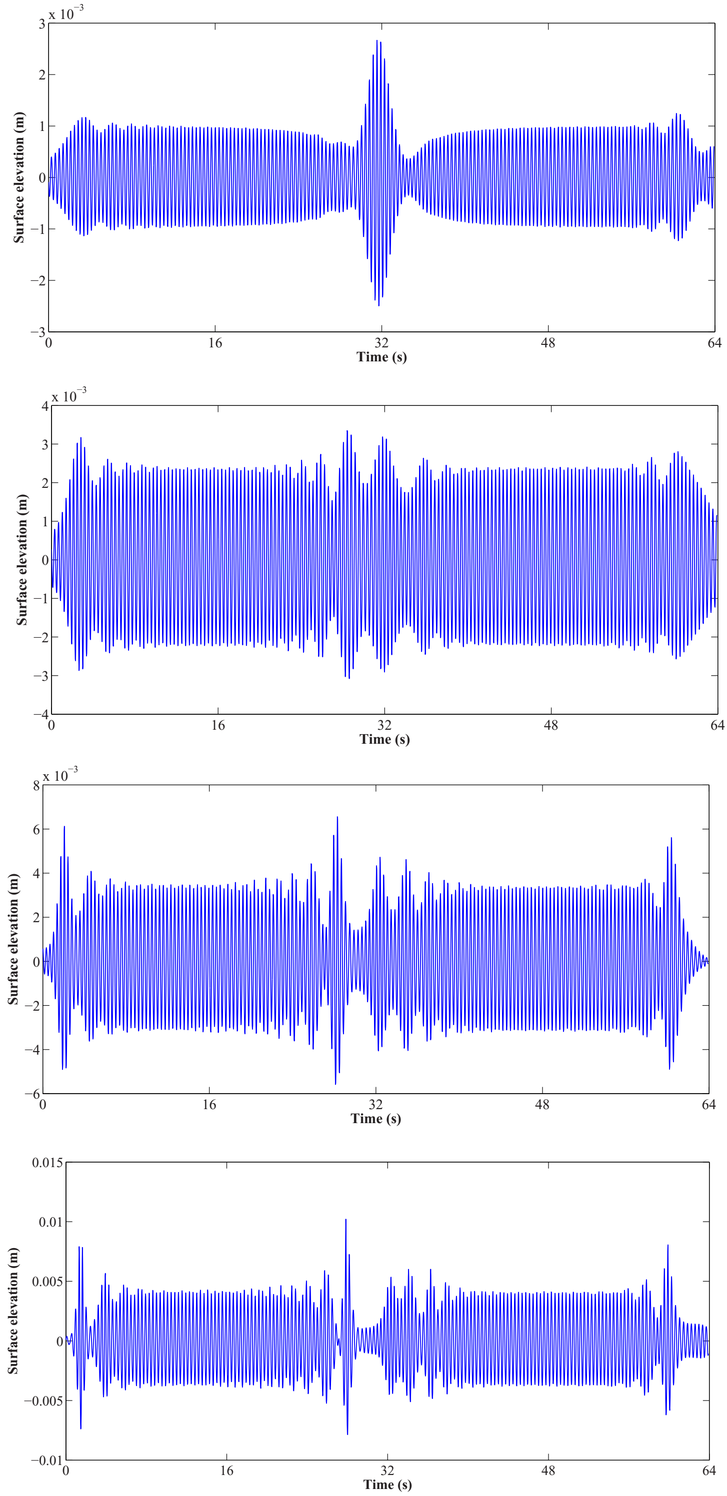

FIG. 14. Probe signal measured after the propagation of the Peregrine breather for $kx_M = 270$ for different steepnesses $ka \in \{0.03, 0.07, 0.10, 0.12\}$ (from top to bottom).

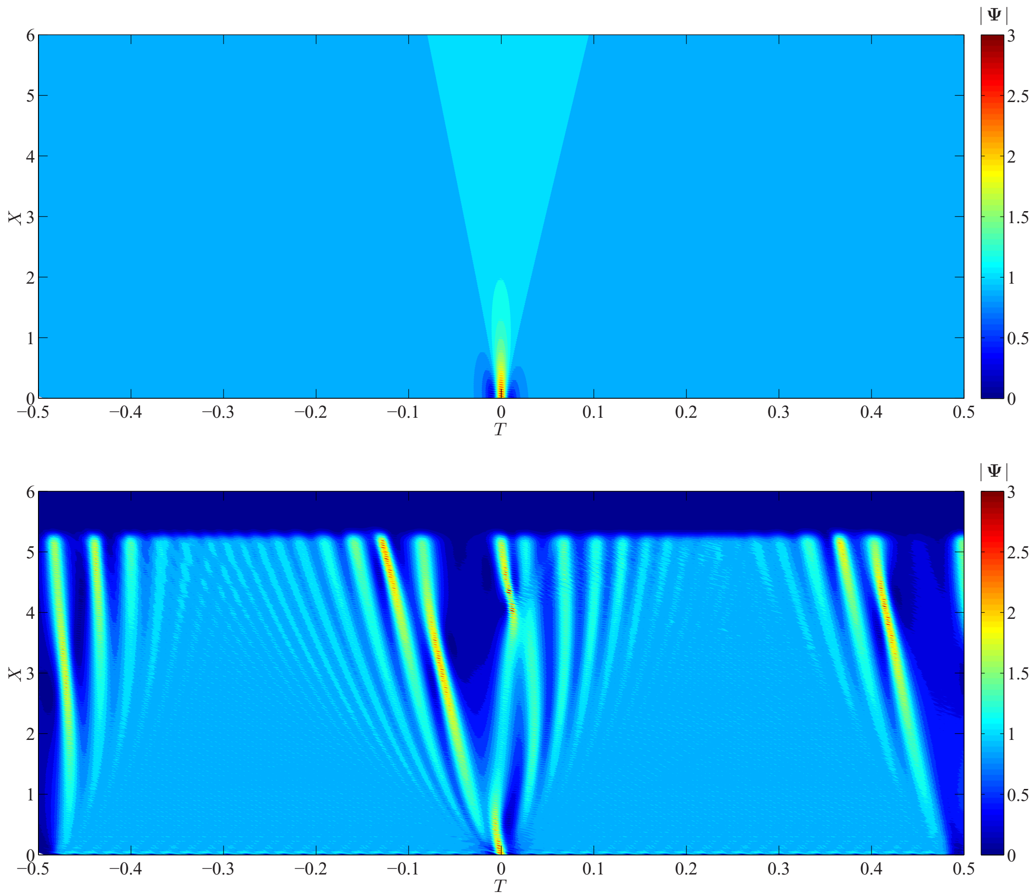

FIG. 15. Space and time evolution of the Peregrine breather for $ka = 0.12$ in the NWT: comparison of the analytic solution (top) and the HOS NWT numerical simulation (bottom).

accordingly. Indeed, we recall that the modulation instability, which drives the evolution of the breather solution, acts on a spatial scale $kx_{\mathrm{BF}} = O(1/(ka)^2)$. Figure 14 presents the probe signals after first propagation of a Peregrine breather at a fixed distance $kx_M = 270$ for different initial steepnesses in the range $ka \in \{0.03, 0.07, 0.10, 0.12\}$.

As expected and shown, the relative propagating distance is different with respect to the breather demodulation, evolving on the time scale $1/(ka)^2$. Consequently, the amplitude decrease of the initial localized structure is highly dependent on this initial steepness [43]. At low steepness, the fixed propagation distance kx_M appears as very small with respect to the modulation distance: The demodulation is less significant and it is expected that the refocusing is more accurate. In contrast, when the steepness is larger, this chosen distance appears to become large with respect to the modulation instability distance. As a consequence, and due to the significance of the nonlinear processes, the solution can appear as highly complex since those high-order effects prevent us from recovering the plane-wave solution. For details, we refer to Fig. 15, which presents the full space-time plane view of the propagation within the NWT for the steepest case $ka = 0.12$, with the variables changed to NLSE scaled variables as a matter of comparison to the scaled analytic solution.

The complexity of the wave pattern at the final stage of demodulation, as a matter of deviation from the constant background, can be clearly perceived. An increasing steepness leads, as expected,

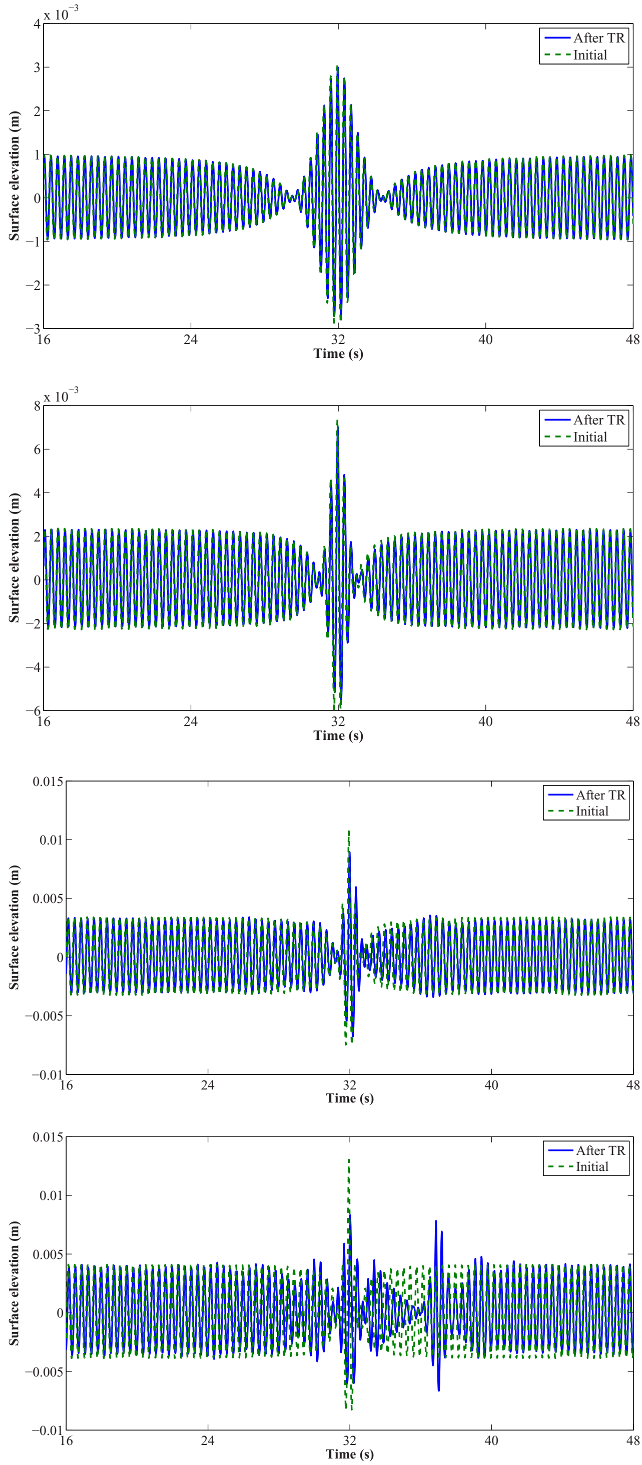

FIG. 16. Comparison of the Peregrine surface profile at maximal compression, as initially generated with respect to the NLSE theory (dashed line) and after TR refocusing (solid line), for $kx_M = 270$ and $ka \in \{0.03, 0.07, 0.1, 0.12\}$ (from top to bottom).

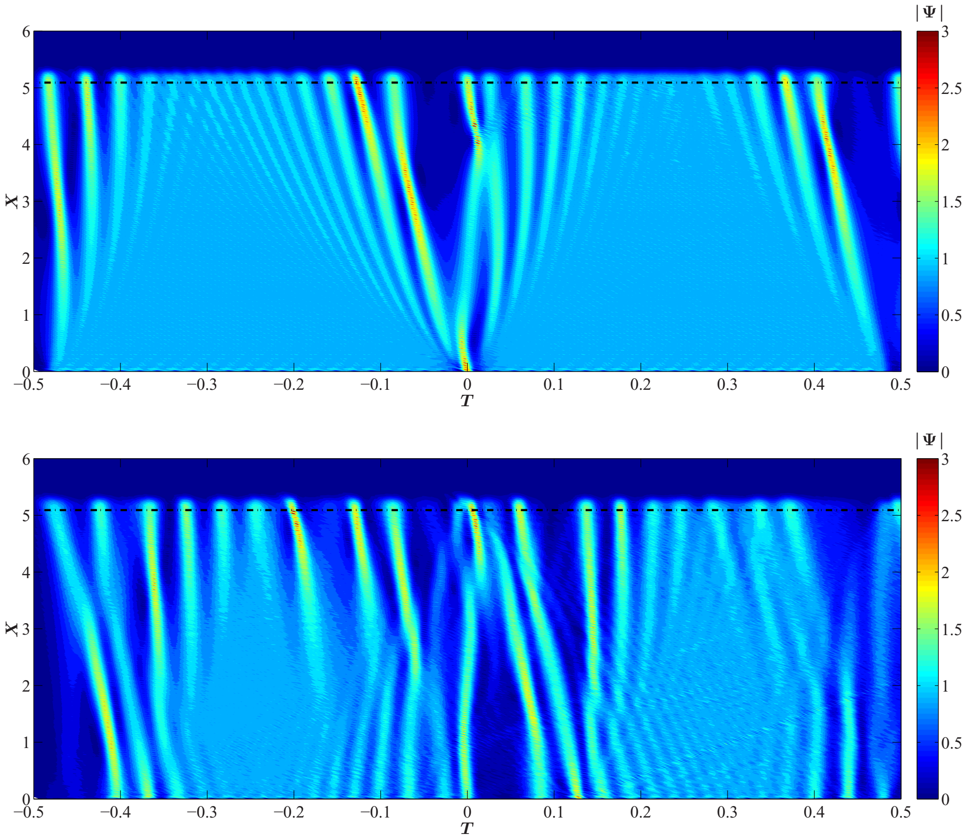

FIG. 17. Space and time evolution of the Peregrine breather for $ka = 0.12$ and $kx_M = 480$ (dash-dotted line) in the NWT: demodulation (top) and TR refocusing (bottom).

to a more complex wave pattern at a fixed location of breather evolution. At the same time, the latter feature is associated with an initial breather modulation that is also quite different when the steepness is changed. As an example, Fig. 16 presents the results obtained after TR refocusing at a fixed location of $kx_M = 270$, as in the previous case, with varying steepness values, in the range $ka \in \{0.03, 0.07, 0.10, 0.12\}$.

It can be noticed that at a fixed time frame duration, when the steepness is lower, the initial breather appears indeed to be wider. The nonlinearity increases the focusing intensity of the initial localized structure by decreasing the breather's lifetime [43]. The free surface profile with respect to the TR refocusing is almost identical to the analytic solution when the steepness is lower than $ka \simeq 0.09$. The increase of the steepness is associated with an increase of deviation in terms of phase shifts. This is similar to what has been observed previously in the dependence study with respect to kx_M. The general behavior of the accuracy with respect to this parameter observed in Fig. 8 is consequently clear.

However, it is important to note that at the largest steepness, the wave field after time-reversal is completely different from the original one. The breather initial structure is completely distorted after the first propagation, as shown in Fig. 14, and is not refocused during the second propagation after time-reversal. When the considered breather exhibits high nonlinearities, the wave field does not tend to the plane-wave solution: Successive highly nonlinear groups are created during the propagation. This feature is associated with both high-order dispersive effects and high-order nonlinearities. These are at play during both propagations and when associated with the chosen wave generation process, they are shown to prevent time-reversibility and consequently limit the application range of the TR technique.

Figure 17 shows the space-time view of the TR procedure for the case $ka = 0.12$ and $kx_M = 480$. The corresponding scaled propagating distance $X_M \simeq 5.0$ is depicted as well.

Clearly, the TR technique is failing and is not valid in this configuration; it is shown that the breaking of time-reversibility of the phenomena studied appears obvious within this framework. From the beginning of the TR refocusing, noticeable differences can be observed between both propagations, pointing out the importance of the wave generation in the TR procedure.

In conclusion, the refocusing of extreme waves with time-reversal exhibits some limitations. The main parameters in this regard are the nonlinearity of the considered wave field and the considered propagating distance. Nevertheless, as shown in Figs. 8 and 9, the applicability of the process is valid for a wide range of realistic parameter choices and is efficient up to a high local steepness of the wave pattern and very long propagating distances.

VI. CONCLUSION

We have reported a detailed numerical study of the applicability of TR mirrors to water waves. A highly nonlinear numerical model based on the HOS method has been set up to reproduce the complete physical configuration of wave generation in a unidirectional NWT: generation of waves by means of a wave maker, absorption of reflecting waves through a beach, etc. The corresponding HOS NWT has been validated with experimental results presented in Ref. [23]. This numerical setup enables us to successfully apply the TR method to refocus different analytic solutions of the NLSE, namely, the stationary envelope soliton and doubly localized Peregrine-type breathers of first and second-order. Note that the time symmetry can be also used to optimize initial conditions for an accurate focusing of water waves [27].

The applicability of the TR procedure has been assessed over a wide range of propagating distances kx_M and initial wave steepness ka, beyond laboratory limitations. Focusing our attention on pulsating solutions (breathers), the study has demonstrated that the TR procedure will allow an accurate TR refocusing of the wave field at a given propagating distance when the local steepness of the localized structures does not exceed a given threshold with respect to the propagation distances. We identified that an accurate TR refocusing is achieved for $kx_M \simeq 270$ and a corresponding local steepness up to $ka \simeq 0.27$. Changing the propagating distance will obviously induce a different threshold.

At the same time, the refocusing of extreme waves with respect to time-reversal exhibits some limitations. The time-reversibility of water-wave propagation appears to be improper for large steepness and large propagating distances. The practical TR procedure for water waves in the configuration of a wave basin relies on some assumptions resulting in this loss of reversibility. Primarily, this is due to the use of the only free surface elevation for time-reversal associated with the approximation of a linear conversion between free surface elevation and the wave maker's motion. These will induce small discrepancies in the generated sea state at the wave maker's location (which are obviously larger with larger nonlinearity). Then the high-order nonlinearities and dispersive effects associated with the wave propagation will induce possible large discrepancies in the final TR refocusing. The applicability of the method is consequently driven by those two parameters, namely, ka and kx_M. The present study has shown these two parameters are closely linked in describing the limitations of the TR technique with respect to the modulation instability length scales in the case of breathers.

Nevertheless, the applicability of the time-reversal to nonlinear waves for the quantified applicability range is quite remarkable, taking into account the laboratory and the numerical noise and dissipation effects, always present, when performing numerical and laboratory tests. Furthermore, we emphasize the importance of this study with respect to the robustness of the TR technique to chaotic motion of the water-wave field, which is known to arise in the context of modulation instability [49,50].

Finally, we emphasize that future interdisciplinary work may be motivated by these results. It is well known that the NLSE describes the propagation of waves in a wide range of nonlinear dispersive media [5,7,8,51]. Furthermore, the reproduction of RWs in wave basins is of significant interest in ocean engineering and has been shown to be very complicated with classical methods [40]. The idea is to reconstruct oceanic extreme waves, such as the New Year Wave, often used as a dedicated model for RWs in the ocean [52]. It is also important to address multidirectionality and irregular wave conditions in order to accurately assert the validity and limitation of the time-reversal in these conditions.

---

[1] G. G. Stokes, On the theory of oscillatory waves, Trans. Cambridge Philos. Soc. **8**, 441 (1847).

[2] C. C. Mei, *The Applied Dynamics of Ocean Surface Waves* (World Scientific, Singapore, 1983), Vol. 1.

[3] T. B. Benjamin and J. E. Feir, The disintegration of wave trains on deep water part 1. Theory, J. Fluid Mech. **27**, 417 (1967).

[4] A. Chabchoub, N. P. Hoffmann, and N. Akhmediev, Rogue Wave Observation in a Water Wave Tank, Phys. Rev. Lett. **106**, 204502 (2011).

[5] B. Kibler, J. Fatome, C. Finot, G. Millot, F. Dias, G. Genty, N. Akhmediev, and J. M. Dudley, The Peregrine soliton in nonlinear fibre optics, Nat. Phys. **6**, 790 (2010).

[6] D. R. Solli, C. Ropers, P. Koonath, and B. Jalali, Optical rogue waves, Nature (London) **450**, 1054 (2007).

[7] M. Onorato, S. Residori, U. Bortolozzo, A. Montina, and F. T. Arecchi, Rogue waves and their generating mechanisms in different physical contexts, Phys. Rep. **528**, 47 (2013).

[8] J. M. Dudley, F. Dias, M. Erkintalo, and G. Genty, Instabilities, breathers and rogue waves in optics, Nat. Photon. **8**, 755 (2014).

[9] V. E. Zakharov, Stability of periodic waves of finite amplitude on the surface of a deep fluid, J. Appl. Mech. Tech. Phys. **9**, 190 (1968).

[10] C. Kharif and E. Pelinovsky, Physical mechanisms of the rogue wave phenomenon, Eur. J. Mech. B **22**, 603 (2003).

[11] A. Osborne, *Nonlinear Ocean Waves & the Inverse Scattering Transform* (Academic, New York, 2010), Vol. 97.

[12] N. J. Zabusky and M. D. Kruskal, Interaction of "Solitons" in a Collisionless Plasma and the Recurrence of Initial States, Phys. Rev. Lett. **15**, 240 (1965).

[13] H. C. Yuen and B. M. Lake, Nonlinear dynamics of deep-water gravity waves, Adv. Appl. Mech. **22**, 67 (1982).

[14] A. Chabchoub, N. Hoffmann, M. Onorato, A. Slunyaev, A. Sergeeva, E. Pelinovsky, and N. Akhmediev, Observation of a hierarchy of up to fifth-order rogue waves in a water tank, Phys. Rev. E **86**, 056601 (2012).

[15] A. Chabchoub, B. Kibler, J. M. Dudley, and N. Akhmediev, Hydrodynamics of periodic breathers, Philos. Trans. R. Soc. London A **372**, 20140005 (2014).

[16] A. Slunyaev, E. Pelinovsky, A. Sergeeva, A. Chabchoub, N. Hoffmann, M. Onorato, and N. Akhmediev, Super-rogue waves in simulations based on weakly nonlinear and fully nonlinear hydrodynamic equations, Phys. Rev. E **88**, 012909 (2013).

[17] M. Fink, Time reversal of ultrasonic fields. I. Basic principles, IEEE Trans. Ultrason. Ferroelectr. Freq. Control **39**, 555 (1992).

[18] P. Roux and M. Fink, Time reversal in a waveguide: Study of the temporal and spatial focusing, J. Acoust. Soc. Am. **107**, 2418 (2000).

[19] R. K. Ing and M. Fink, Time-reversed Lamb waves, IEEE Trans. Ultrason. Ferroelectr. Freq. Control **45**, 1032 (1998).

[20] M. Tanter, J.-L. Thomas, F. Coulouvrat, and M. Fink, Breaking of time reversal invariance in nonlinear acoustics, Phys. Rev. E **64**, 016602 (2001).

[21] A. Przadka, S. Feat, P. Petitjeans, V. Pagneux, A. Maurel, and M. Fink, Time Reversal of Water Waves, Phys. Rev. Lett. **109**, 064501 (2012).
[22] V. Bacot, M. Labousse, A. Eddi, M. Fink, and E. Fort, Time reversal and holography with spacetime transformations, Nat. Phys. (2016), doi: 10.1038/nphys3810.
[23] A. Chabchoub and M. Fink, Time-Reversal Generation of Rogue Waves, Phys. Rev. Lett. **112**, 124101 (2014).
[24] G. Ducrozet, F. Bonnefoy, D. Le Touzé, and P. Ferrant, A modified high-order spectral method for wavemaker modeling in a numerical wave tank, Eur. J. Mech. B **34**, 19 (2012).
[25] B. J. West, K. A. Brueckner, R. S. Janda, D. M. Milder, and R. L. Milton, A new numerical method for surface hydrodynamics, J. Geophys. Res. Oceans **92**, 11803 (1987).
[26] D. G. Dommermuth and D. K. P. Yue, A high-order spectral method for the study of nonlinear gravity waves, J. Fluid Mech. **184**, 267 (1987).
[27] L. Shemer, K. Goulitski, and E. Kit, Evolution of wide-spectrum unidirectional wave groups in a tank: An experimental and numerical study, Eur. J. Mech. B **26**, 193 (2007).
[28] G. Ducrozet, F. Bonnefoy, D. Le Touzé, and P. Ferrant, 3-D HOS simulations of extreme waves in open seas, Nat. Hazards Earth Syst. Sci. **7**, 109 (2007).
[29] A. V. Slunyaev and V. I. Shrira, On the highest non-breaking wave in a group: Fully nonlinear water wave breathers versus weakly nonlinear theory, J. Fluid Mech. **735**, 203 (2013).
[30] S. Nazarenko, *Wave Turbulence* (Springer Science & Business Media, New York, 2011), Vol. 825.
[31] V. E. Zakharov and A. B. Shabat, Exact theory of two-dimensional self-focusing and one-dimensional self-modulation of waves in nonlinear media, Sov. Phys. JETP **34**, 62 (1972).
[32] D. H. Peregrine, Water waves, nonlinear Schrödinger equations and their solutions, J. Aust. Math. Soc. Ser. B **25**, 16 (1983).
[33] N. Akhmediev, V. M. Eleonskii, and N. E. Kulagin, Generation of periodic trains of picosecond pulses in an optical fiber: Exact solutions, Sov. Phys. JETP **62**, 894 (1985).
[34] V. I. Shrira and V. V. Geogjaev, What makes the Peregrine soliton so special as a prototype of freak waves? J. Eng. Math. **67**, 11 (2010).
[35] N. Akhmediev, A. Ankiewicz, and M. Taki, Waves that appear from nowhere and disappear without a trace, Phys. Lett. A **373**, 675 (2009).
[36] See Supplemental Material at http://link.aps.org/supplemental/10.1103/PhysRevFluids.1.054302 for the details about the analytic solutions to NLSE, the numerical model and parameters, and the validation results.
[37] A. Toffoli, O. Gramstad, K. Trulsen, J. Monbaliu, E. Bitner-Gregersen, and M. Onorato, Evolution of weakly nonlinear random directional waves: Laboratory experiments and numerical simulations, J. Fluid Mech. **664**, 313 (2010).
[38] A. Toffoli, M. Onorato, E. M. Bitner-Gregersen, and J. Monbaliu, Development of a bimodal structure in ocean wave spectra, J. Geophys. Res. Oceans **115**, 1 (2010).
[39] C. Kharif, E. Pelinovsky, and A. Slunyaev, *Rogue Waves in the Ocean* (Springer, Berlin, 2009).
[40] G. Ducrozet, F. Bonnefoy, and P. Ferrant, On the equivalence of unidirectional rogue waves detected in periodic simulations and reproduced in numerical wave tanks, Ocean Eng. **117**, 346 (2016).
[41] A. Slunyaev, G. F. Clauss, M. Klein, and M. Onorato, Simulations and experiments of short intense envelope solitons of surface water waves, Phys. Fluids **25**, 067105 (2013).
[42] D. Clamond, M. Francius, J. Grue, and C. Kharif, Long time interaction of envelope solitons and freak wave formations, Eur. J. Mech. B **25**, 536 (2006).
[43] A. Chabchoub, N. Akhmediev, and N. P. Hoffmann, Experimental study of spatiotemporally localized surface gravity water waves, Phys. Rev. E **86**, 016311 (2012).
[44] K. Trulsen and K. B. Dysthe, A modified nonlinear Schrödinger equation for broader bandwidth gravity waves on deep water, Wave Motion **24**, 281 (1996).
[45] E. Lo and C. C. Mei, A numerical study of water-wave modulation based on a higher-order nonlinear Schrödinger equation, J. Fluid Mech. **150**, 395 (1985).
[46] A. Chabchoub, N. Hoffmann, M. Onorato, G. Genty, J. M. Dudley, and N. Akhmediev, Hydrodynamic Supercontinuum, Phys. Rev. Lett. **111**, 054104 (2013).

[47] L. Shemer and L. Alperovich, Peregrine breather revisited, Phys. Fluids **25**, 051701 (2013).

[48] H. A. Schäffer, Second-order wavemaker theory for irregular waves, Ocean Eng. **23**, 47 (1996).

[49] E. A. Caponi, P. G. Saffman, and H. C. Yuen, Instability and confined chaos in a nonlinear dispersive wave system, Phys. Fluids **25**, 2159 (1982).

[50] T. Yasuda and N. Mori, Roles of sideband instability and mode coupling in forming a water-wave chaos, Wave Motion **26**, 163 (1997).

[51] J. M. Dudley, G. Genty, F. Dias, B. Kibler, and N. Akhmediev, Modulation instability, Akhmediev breathers and continuous wave supercontinuum generation, Opt. Express **17**, 21497 (2009).

[52] S. Haver, A possible freak wave event measured at the Draupner Jacket January 1 1995, in *Proceedings of Rogue Waves, Brest, France*, edited by M. Olagnon and M. Prevosto (IFREMER, Brest, 2004).